

A Brief Overview of Silicon Nanoparticles as Anode Material: A Transition from Lithium-Ion to Sodium-Ion Batteries

Alireza Fereydooni, Chenghao Yue, and Yimin Chao*

The successful utilization of silicon nanoparticles (Si-NPs) to enhance the performance of Li-ion batteries (LIBs) has demonstrated their potential as high-capacity anode materials for next-generation LIBs. Additionally, the availability and relatively low cost of sodium resources have a significant influence on developing Na-ion batteries (SIBs). Despite the unique properties of Si-NPs as SIBs anode material, limited study has been conducted on their application in these batteries. However, the knowledge gained from using Si-NPs in LIBs can be applied to develop Si-based anodes in SIBs by employing similar strategies to overcome their drawbacks. In this review, a brief history of Si-NPs' usage in LIBs is provided and discuss the strategies employed to overcome the challenges, aiming to inspire and offer valuable insights to guide future research endeavors.

high energy density, satisfactory working potential, superior cycling stability, and eco-friendliness. The most popular of these are sodium-ion batteries (SIBs) and lithium-ion batteries (LIBs).^[5] It has been well versed in the literature that electrode materials, particularly anode materials, provide great potential for improving battery energy density as compared to cathode materials in both LIBs and SIBs.^[6–9] In a general view, anode materials can be divided into three categories based on their ion storage mechanism: 1) intercalation (also known as insertion),^[10,11] 2) alloying,^[12–15] and 3) conversion.^[14–17]

Anodes for commercial LIBs are primarily made of intercalating graphite, which has a theoretical capacity of $\approx 370 \text{ mAhg}^{-1}$

for LiC_6 .^[18] Nevertheless, graphite has been considered as thermodynamically unfavorable intercalating medium for SIBs (namely $\text{NaC}_6/\text{NaC}_8$).^[19] Also, theoretical calculations demonstrated a reversible capacity of $\approx 35 \text{ mAhg}^{-1}$ for NaC_{64} .^[20] This low capacity is ascribed to certain accountable factors, such as the larger ionic radius of Na^+ (1.06 Å) compared to Li^+ (0.76 Å) which hampers the ionic intercalation process.^[21–24] As an alternative, other carbonaceous materials with wider interlayer spacings have been introduced for intercalation-type SIBs anodes, among which hard carbon has drawn considerable attention in this area.^[25] Many attempts have been made to increase hard carbon's capacity in Na storage, from the choice of precursor,^[26–28] to optimizing the operating conditions;^[29–34] yet its capacity is still insufficient for large-scale applications. Carbonaceous anodes also have a relatively low reaction potential with Li and Na, which results in Li and Na dendritic deposition during battery's charge/discharge cycles, and thus raises safety concerns such as short circuiting.^[35]

Conversion-type anode materials offer much higher capacities than carbonaceous compounds. Several studies have investigated the use of conversion-based compounds as anode material.^[36–41] Despite their ultra-high capacity, their widespread application has been severely hampered by their low conductivity and poor cycling stability.^[16,42]

Alloying materials in LIBs and SIBs have recently received enormous attention due to their higher capacity, lower cost and safer performance compared to intercalation- and conversion-type anodes. Alloy-type anode materials undergo the following electrochemical reactions $\text{M} + x\text{N} \rightleftharpoons \text{N}_x\text{M}$ where N is the host alkaline element (i.e., lithium or sodium) and M is the alloying agent. The most common metals and metalloids used as alloying-type anodes are silicon (Si), germanium (Ge), antimony (Sb), tin

1. Introduction

Global warming, dwindling fossil fuel reserves, and the urgent need for decarbonizing electric power sector have prompted considerable attention to renewable energies. To use renewable energies as a stable and reliable source in daily-life applications, high-performance energy storage devices need to be implemented in electric grids, electric vehicles (EVs), mobile electronics and other electricity-driven devices.^[1–4] In recent years, there has been a growing adoption of batteries composed of group 1 and 2 metals (e.g., alkaline, and alkaline earth elements) thanks to their

A. Fereydooni, C. Yue, Y. Chao

School of Chemistry
University of East Anglia
Norwich, NR4 7TJ, UK
E-mail: Y.Chao@uea.ac.uk

A. Fereydooni
Tyndall Center for Climate Change Research
University of East Anglia
Norwich, NR4 7TJ, UK

Y. Chao
National energy key laboratory for new hydrogen-ammonia
energy technologies
Foshan Xianhu Laboratory
Foshan 528200, China

 The ORCID identification number(s) for the author(s) of this article can be found under <https://doi.org/10.1002/smll.202307275>

© 2023 The Authors. Small published by Wiley-VCH GmbH. This is an open access article under the terms of the Creative Commons Attribution License, which permits use, distribution and reproduction in any medium, provided the original work is properly cited.

DOI: 10.1002/smll.202307275

Table 1. Electrochemical properties of common alloying anode materials.

Element	Alloying Compound	Theoretical Capacity (mAh g ⁻¹) [44–48]	Volume Expansion (%) ^[44–47,49]	Volumetric capacity (mAh cm ⁻³) ^[5,43,45]	Conductivity (S cm ⁻¹) ^[5,44]	Density (g cm ⁻³) ^[5,45]	Terrestrial Abundance (%) ^[50]	Annual Extraction (ton) ^[51]
Si	Li ₂₂ Si ₅	4200	400	–	2.52 × 10 ⁻⁶	2.33	28.2	7.20 × 10 ⁶
	NaSi	954	114	2190	–	–	–	–
Ge	Li ₂₂ Ge ₅	1624	370	–	1.45 × 10 ⁻²	5.32	1.5 × 10 ⁻⁴	3.65 × 10 ⁴
	NaGe	369	300	1624	–	–	–	–
Sb	Li ₃ Sb	660	200	–	2.88 × 10 ⁴	6.68	2 × 10 ⁻⁵	1.30 × 10 ⁵
	Na ₃ Sb	660	390	660	–	–	–	–
Sn	Li ₂₂ Sn ₅	994	340	–	9.50 × 10 ⁴	7.31	2.3 × 10 ⁻⁴	2.80 × 10 ⁵
	Na ₁₅ Sn ₄	847	423	994	–	–	–	–
Bi	Li ₃ Bi	385	200	–	8.67 × 10 ³	9.75	8.5 × 10 ⁻⁷	1.02 × 10 ⁴
	Na ₃ Bi	385	250	3800	–	–	–	–

(Sn), and bismuth (Bi).^[5,43] **Table 1** summarizes their key characteristics. A graphical comparison of the investigated characteristics for the above-mentioned elements in SIBs is depicted in **Figure 1a**, where 5 represents the highest scale (most favorable) and 1 represents the lowest (least favorable). Values are normalized based on the maximal and minimal results tabulated in **Table 1**. Theoretical capacity as well as volume expansion during alloying in LIBs and SIBs are separately compared in **Figure 1b,c**, respectively.

Among these compounds, Si exhibits the highest theoretical capacity both in LIBs and SIBs. Furthermore, considering its abundant resources, high extraction, low working potential, and environmentally friendly nature, Si has long been known to be one of the most promising anode material for LIBs, and numerous studies have successfully investigated its application in high-performance LIBs.^[52–56] Despite Si's theoretical capacity being

the highest and its volume expansion being the smallest among alloying-type SIB anode compounds, not many researchers have focused on its implementation in high-performance SIBs. The scarcity of Si-based anodes for SIBs may be attributable to the fact that SIBs have only recently regained popularity. Moreover, Si anodes are plagued by severe volume fluctuations during charge/discharge cycles, which causes serious pulverization of the anode materials and eventually leads to capacity degradation and poor cyclability.^[57,58] Retrospectively, when considering the history of Si as an anode material for LIBs, it is apparent how nanoengineering has alleviated these concerns; designing nano-scaled structured alloys can result in high gravimetric capacities and rates, superior fracture endurance, smaller ionic diffusion paths, as well as mitigated volume expansion.^[58–61] Our objective in this review is to recount a brief history of the use of Si-NPs in LIBs along with the strategies used to tackle the challenges, so

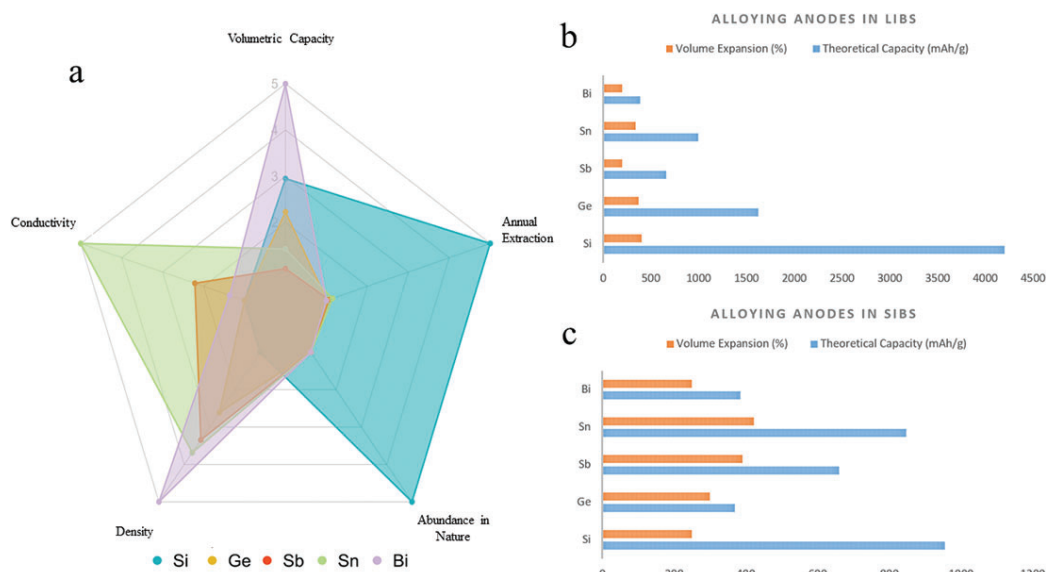


Figure 1. a) Comparison of common alloying-type elements used as anode materials in SIBs, b,c) theoretical capacity and volume expansion of alloying-type anodes in LIBs and SIBs.

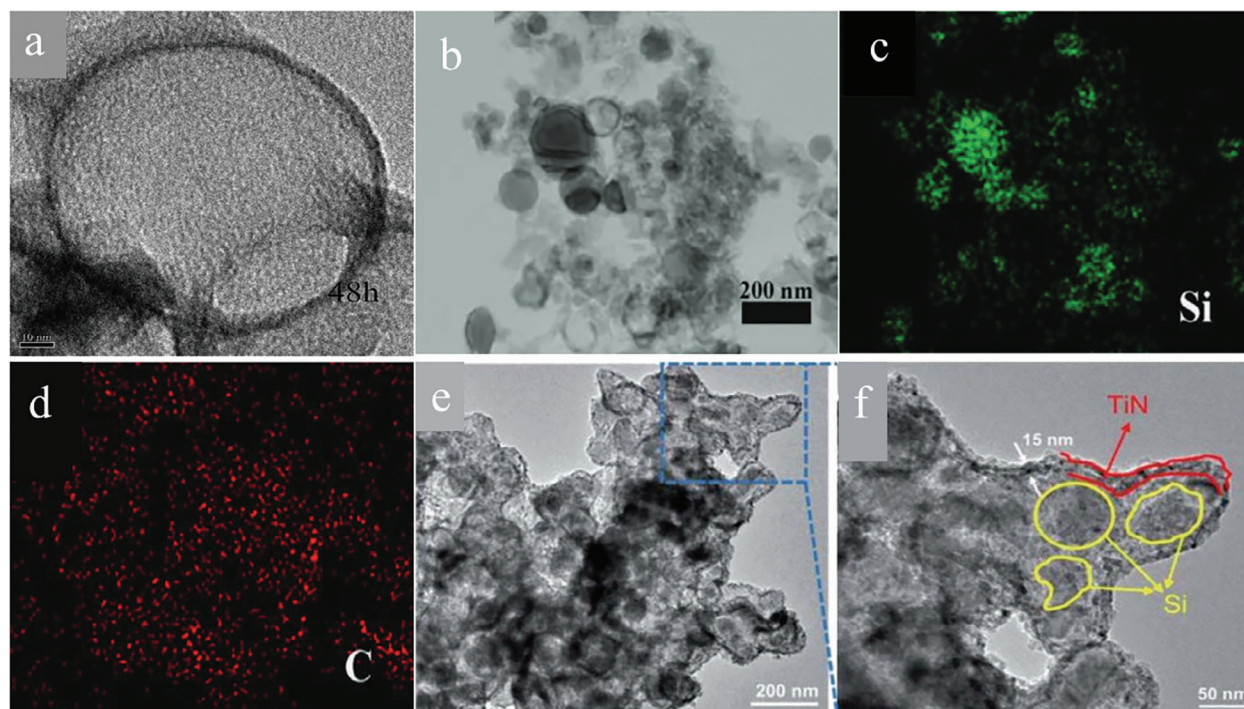


Figure 2. a) TEM image of hollow Si@C after 48 h of HF etching. Reprinted with permission.^[62] Copyright 2015, Royal Society of Chemistry. b–d) STEM image of Si@void@C/C and corresponding elemental mapping of Si and C. Reprinted with permission.^[63] Copyright 2021, John Wiley and Sons. e, f) STEM image of Si@TiN. Reprinted under terms of the CC-BY-NC 3.0 license.^[64] Copyright 2022, Royal Society of Chemistry.

that inspirations and insights can be gained into their application in SIBs and potentially other types of batteries like potassium-ion batteries.

2. Silicon in Lithium-Ion Batteries

It has long been known that the downside to Si-based LIBs anodes is that they suffer from low conductivity ($\approx 10^{-5}$ S cm⁻¹), sluggish ion diffusion kinetics ($\approx 10^{-14}$ cm² s⁻¹), and drastic volume fluctuations during the lithiation-delithiation process ($\approx 400\%$), which eventually mitigate battery's electrochemical performance.^[55–57]

Researchers have developed innovative nanostructures in an attempt to mitigate these drawbacks. As an example, Pang et al.^[62] synthesized a hollow Si@C nanostructure (Figure 2a) via carbonizing the emulsified polyacrylonitrile (PAN) at 1000 °C for 2 h with a heating rate of 10 °C min⁻¹ followed by HF etching. This nanocomposite retained a specific capacity of 700 mAhg⁻¹ at 0.25 Ag⁻¹ after 100 cycles. More recently, Ma et al.^[63] synthesised a yolk-shell structure of Si@void@C nanoparticles embedded in 3D carbon-net (Figure 2b–d). Their preparation method involved UV illumination to a microemulsion of water and oil, followed by freeze drying and hydrothermal treatment. The yolk-shell structure delivered a high capacity of 1160 mAhg⁻¹ at 0.3 Ag⁻¹ after 300 cycles. The excellent performance of such hollow structure's bears witness to their effectiveness in buffering the volume expansion of bare silicon. More recently, Zhang et al.^[64] used titanium nitride (TiN) as a coating layer (Figure 3a) to develop a yolk-shell-like Si@TiN nanocomposite (Figure 2e,f). Their proposed composite exhibited a re-

versible capacity of 2047 mAhg⁻¹ at 1 Ag⁻¹ after 180 cycles and a remarkable discharge capacity of 903 mAhg⁻¹ at high current density of 12 Ag⁻¹ (Figure 3b–d). This special yolk-shell configuration not only accommodates the volumetric expansion of Si-NPs in recurrent cycling, but also boosts the electronic conductivity of pure Si, thanks to the conductive TiN shell, leading to its notable cyclic performance.

It is important to note, however, that despite the effectiveness of such nanocomposites in mitigating anode volume expansion, they cannot yet be mass produced at a substantial scale. Many factors contribute to this, including high production costs and low initial Columbic efficiency (ICE). The low ICE stems from nanomaterials' interaction with electrolytes because of their high specific surface areas.^[65–69]

Recent years have witnessed the development of several strategies to minimize manufacturing costs, mainly by substituting inexpensive substitutes for bare silicon. The following sections provide an overview of these strategies and materials.

2.1. Silicon Monoxide

Due to their extremely abundant resources, low cost, ease of synthesis, and relatively smaller volume change, silicon oxides have been promoted as promising substitutes for elemental Si.^[69] In particular, a majority of attention has been paid to Silicon monoxide (SiO) as an anode material for LIBs. It is also possible to support volume fluctuations and increase anode electrical conductivity by using carbon as a matrix (or scaffold) to reinforce the SiO structure. Ohzuku et al.^[70] developed a SiO/C

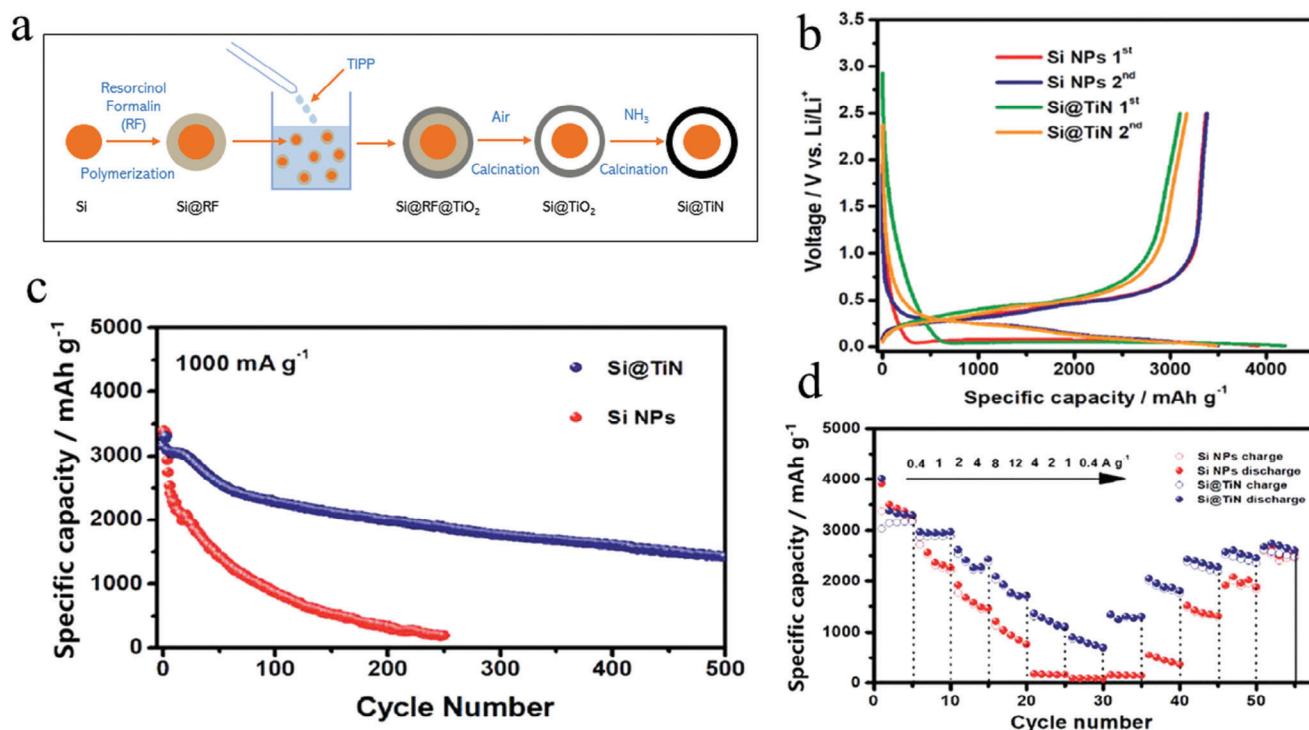


Figure 3. a) Graphical depiction of the synthesis of the yolk–shell Si@TiN composite. Reproduced under terms of the CC-BY-NC 3.0 license.^[64] Copyright 2022, Royal Society of Chemistry. b) The first and second galvanostatic charge/discharge profile, c) cycling performance at a current density of 1 Ag^{-1} , and d) rate performance of the Si-NPs and Si@TiN samples. Reprinted under terms of the CC-BY-NC 3.0 license.^[64] Copyright 2022, Royal Society of Chemistry.

composite (Figure 4a) composed of only 50 wt.% SiO incorporated with carbon fiber (9 wt.%), deposited carbon (20 wt.%), and graphite (21 wt.%). The SiO/C composite demonstrated a 700 mAhg^{-1} discharge capacity after 100 cycles at 0.5 C. Using synthesized composite as the anode in a 14 500 full cell with $\text{LiCo}_{1/3}\text{Ni}_{1/3}\text{Mn}_{1/3}\text{O}_2/\text{LiCoO}_2$ cathode, Ohzuku's group reported a capacity of 200 mAhg^{-1} at 1 Ag^{-1} current density after 300 cycles.^[71] Liu et al.^[72] utilized chemical vapor deposition (CVD) approach to develop SiO coated with graphene (Figure 4b). After 100 cycles, a remarkable capacity of 1600 mAhg^{-1} and an ICE of 95% were reported for this synthesized composite at 0.32 Ag^{-1} . This high specific capacity was attributed to the unique structure of particles, which make stable electrical contacts, facilitated ion diffusion paths, and buffering effect against volume expansion.

A variety of metals and metal oxides have been used in SiO anodes to enhance lithium storage. Wang et al.^[73] used mechanical milling to develop SiO/ Fe_2O_3 composite (Figure 4c). The prepared composite delivered 600 mAhg^{-1} capacity at 4.8 Ag^{-1} current with 71% capacity retention after 50 cycles. Amine et al.^[74] used ultrahigh energy ball milling to develop a state-of-the-art SiO/ $\text{Sn}_x\text{Co}_y\text{C}_z$ anode composite. In particular, 50 wt.% $\text{Sn}_{30}\text{Co}_{30}\text{C}_{40}$ with 50 wt.% SiO combination demonstrated a fairly steady capacity of 900 mAhg^{-1} at 0.3 Ag^{-1} . Substituting Co with Fe, Amine and coworkers later developed a family of SiO/ $\text{Sn}_x\text{Fe}_y\text{C}_z$ composite. It was shown that SiO/ $\text{Sn}_{30}\text{Fe}_{30}\text{C}_{40}$ composite delivers a capacity of 900 mAhg^{-1} at the same current density (0.3 Ag^{-1}).^[75] Miyachi et al.^[76] compared SiO doping with Ti, Ni, and Fe dopants. Their study showcased 84% ICE for Ni

dopant (25 wt.%), as well a remarkable 100% ICE for Li-added Ni doped SiO. In a study done by Yamamura and coworkers,^[77] SiO was uniformly coated with Fe_2SiO_4 at 800°C for 3 h under Ar atmosphere, providing an anode with an 89.3% of ICE.

2.2. Silicon Dioxide (Silica)

The earth's crust consists primarily of silicon dioxide (SiO_2) in its crystalline polymorph form. It has been shown that nanoparticles are necessary to harvest the full theoretical capacity of SiO_2 anodes (1965 mAhg^{-1}).^[78–80] To reduce the size of bulk SiO_2 , Liang et al.^[81] used ball milling over a variety of time periods. The obtained anode from 24 h milled SiO_2 (Figure 5a) delivered a capacity of 602 mAhg^{-1} at 0.1 Ag^{-1} over 150 cycles with $\approx 55\%$ of ICE followed by 99.8% capacity retention (relative to second cycle). SiO_2 has also actively been used in more complex nanostructures. For instance, Favors and coworkers^[82] used hard-template growth approach to fabricate SiO_2 nanotubes (Figure 5b) with 1247 mAhg^{-1} discharge capacity after 100 cycles in response to 0.5 C-rate. Nonetheless, an ICE of 43.3% requires considerable improvement. More recently, Ma et al.^[83] synthesized a hierarchically porous multi-shell hollow SiO_2 structure (Figure 5c) via a sacrificial template method using Na_2SiO_3 as precursor. The obtained hollow spheres then used in anode and delivered a capacity of 750 mAhg^{-1} after 500 cycles at 0.1 Ag^{-1} current density.

Since SiO_2 is the least electrically conductive of the Si oxides, considerable effort has been made to use carbon in conjunction

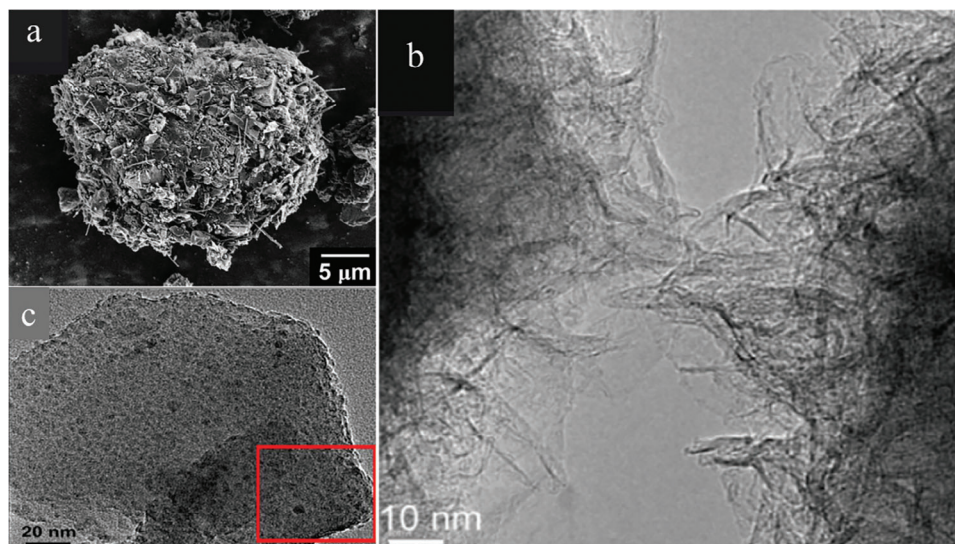


Figure 4. a) SEM image of SiO/C composite. Reprinted with permission.^[70] Copyright 2011, IOPscience. b) TEM image of connected particles of graphene coated on SiO. Reprinted with permission.^[72] Copyright 2017, American Chemical Society. c) HRTEM image of SiO/Fe₂O₃ composite. Reprinted with permission.^[73] Copyright 2013, Elsevier.

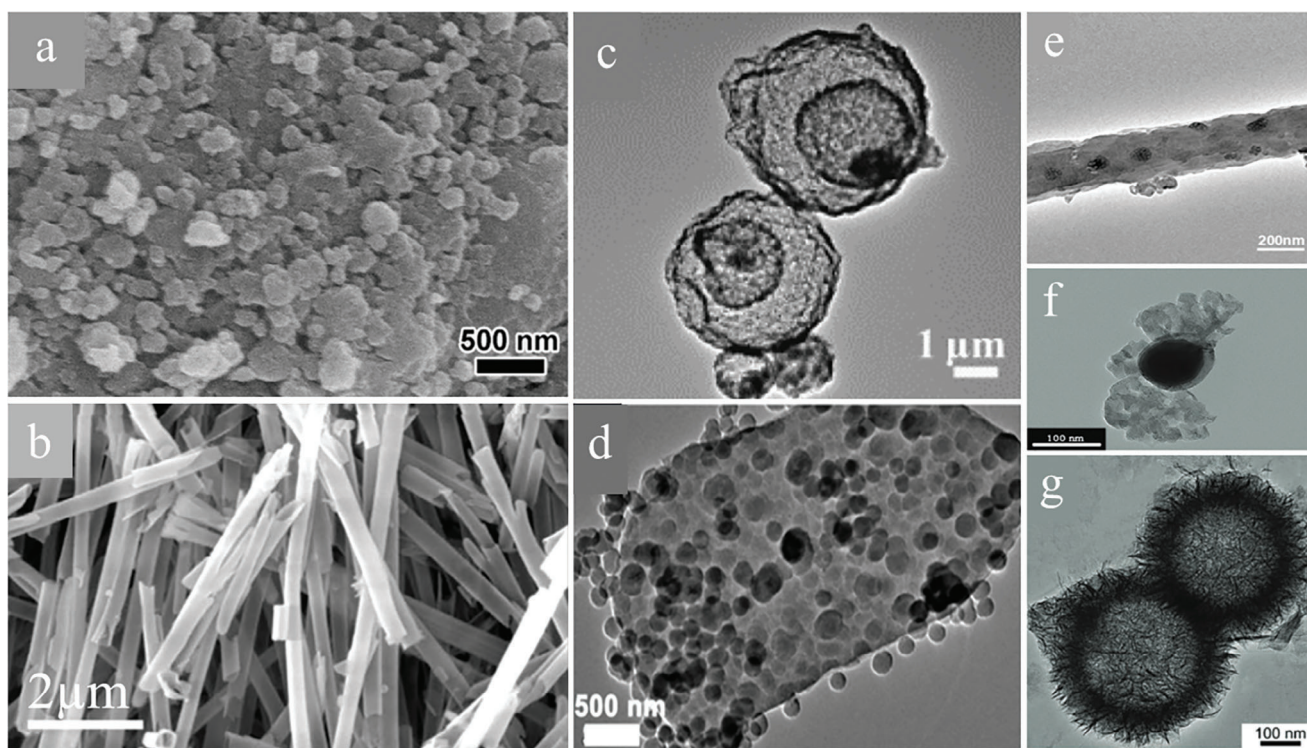


Figure 5. a) FESEM image of the SiO₂ samples with 24 h ball milling. Reprinted with permission.^[81] Copyright 2017, Elsevier. b) SEM image of SiO₂ nano tubes. Reprinted under terms of the CC license.^[82] Copyright 2014, Springer Nature. c) TEM image of multi-shell hollow SiO₂ spheres. Reprinted with permission.^[83] Copyright 2017, Elsevier. d) SEM image of plum-pudding like SiO₂/graphite. Reprinted with permission.^[84] Copyright 2015, Royal Society of Chemistry. e) TEM image of SiO₂/C nanofibers. Reprinted with permission.^[85] Copyright 2015, Elsevier. f) TEM image of SiO₂@CYB. Reprinted with permission.^[86] Copyright 2021, John Wiley and Sons. g) TEM image of Ni/SiO₂ hollow spheres. Reprinted with permission.^[87] Copyright 2018, John Wiley and Sons.

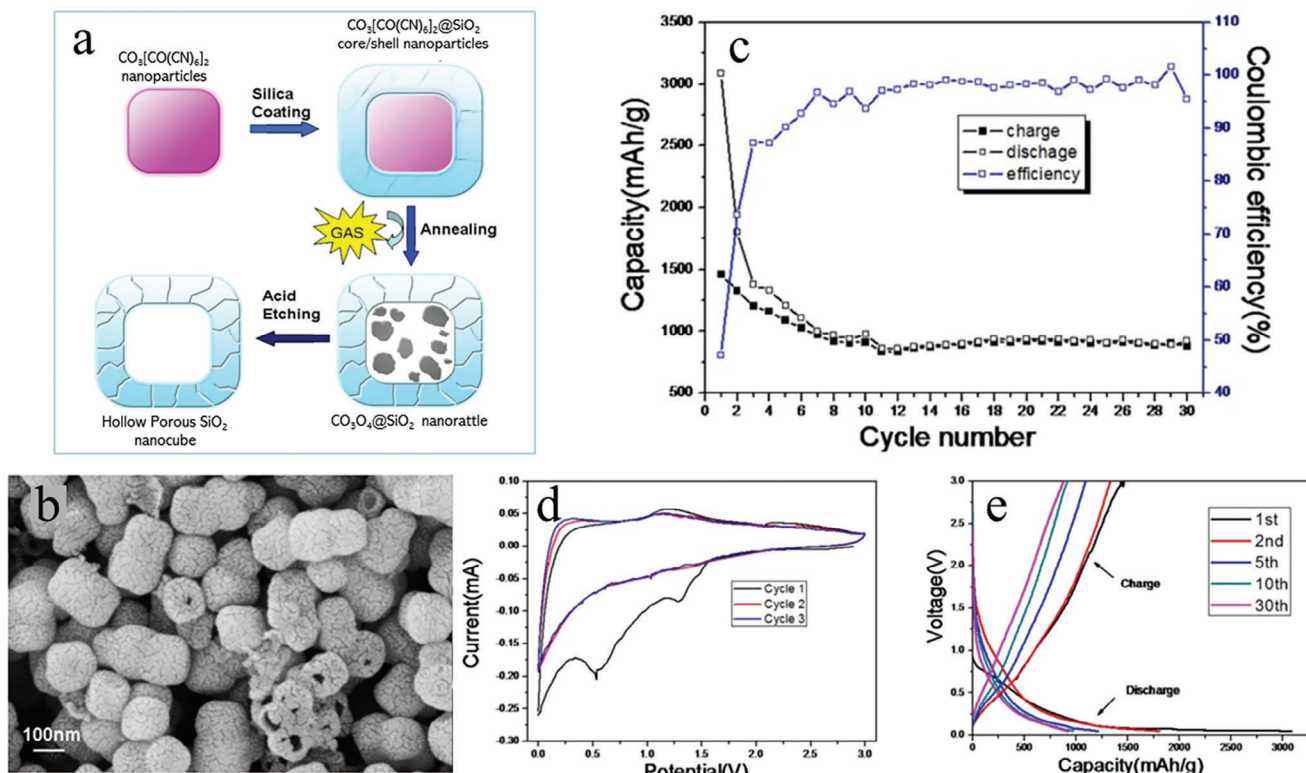


Figure 6. a) Graphical depiction of the synthesis of hollow porous SiO₂ nanocube, and their b) SEM image, c) cycling performance at a current density of 0.1 Ag⁻¹, d) cyclic voltammety between 3 and 0 V at a scan rate of 0.1 mVs⁻¹, and e) galvanostatic discharge/charge profiles. reprinted under terms of the CC-BY license.^[92]

with it.^[84–91] Zhang et al.^[84] synthesized a plum-pudding nanostructure of SiO₂ nanosphere within flake graphite using a hydrothermal process (Figure 5d). Under a current density of 0.1 Ag⁻¹, the prepared composite was reported to exhibit a discharge capacity of 702 mAhg⁻¹ after 100 cycles and a remarkable Coulombic efficiency of 99%. Wu et al.^[85] prepared SiO₂/C nanofibers (Figure 5e) using SiO₂-NPs (≈ 30 nm) incorporated polyacrylonitrile (PAN) through electrospinning, followed by carbonization (800 °C for 2 h and heating rate of 2 °C min⁻¹). Anodes made of nanofibers with 15% silica showed a reversible capacity of 658 mAhg⁻¹ after 100 cycles at 0.05 Ag⁻¹. To improve the reversible capacity of SiO₂ anode materials, Wang et al.^[86] fabricated a yarn-ball structure of nanoscale SiO₂ entangled to carbon wires (Figure 5f) via polycondensation reaction between citric acid and ethylene glycol. The synthesized structure, SiO₂@CYB, has been reported to successfully mitigate the volume fluctuations and enhance the electrical conductivity of SiO₂, which contribute to a first discharge specific capacity of 1297 mAhg⁻¹ at 0.1 Ag⁻¹ current density and ICE of 94%. Nevertheless, it is still unclear what mechanisms lead to the formation of the carbon-yarn-ball structure. Yan et al.^[92] prepared hollow porous SiO₂ nanocubes using a two-step hard-template process (Figure 6a,b). This nanocomposite delivered a reversible capacity of 919 mAhg⁻¹ over 30 cycles (Figure 6c–e), with a relatively stable performance after 12th cycle. The observed characteristic can be linked to the distinct hollow nano-design featuring a spacious interior and multiple pockets in the shell. These features buffer

volume fluctuations and reduce structural stress when Li⁺ move in and out. They also promote quick Li⁺ movement during the charging and discharging process. This research indicates that the creation of either permanent or reversible lithium silicates in the anodes plays a crucial role in determining the deep-cycle battery's capacity. Speedy Li⁺ movement in the hollow porous SiO₂ nanocubes aids in forming Li₂O and Si, leading to the reversible capacity.

It has also been demonstrated that coupling SiO₂ with conductive metal enhances electrochemical activity and electrical conductivity. Zhou et al.^[87] synthesized a novel SiO₂/Ni nanocomposite through reduction of nickel silicate in inert atmosphere (Figure 5g). As a result of its distinctive structural hallmarks, the proposed nanocomposite exhibited a capacity of 672 mAhg⁻¹ at 0.1 Ag⁻¹ after 50 cycles. The same method could also be used to prepare other SiO₂/metal nanocomposites.

As a means of reducing costs and ensuring sustainability, using biomass as a precursor offers many advantages. Li and co-workers^[93] used rice husks (RHs) as a Si-rich biomass to develop a core-shell C@SiO₂ composite. Under a current density of 1 Ag⁻¹, the prepared composite with 38.27 wt.% carbon content delivered a capacity of 534 mAhg⁻¹ after 1000 cycles, which is equivalent to 93% of the capacity of its commercial raw material counterpart. In another work, Li et al.^[94] added magnesianthermic reduction and additives modification to the extracted lignin-SiO₂ from RHs. They reported a first discharge capacity of 2560 mAhg⁻¹ at 0.1 Ag⁻¹. This remarkable capacity was

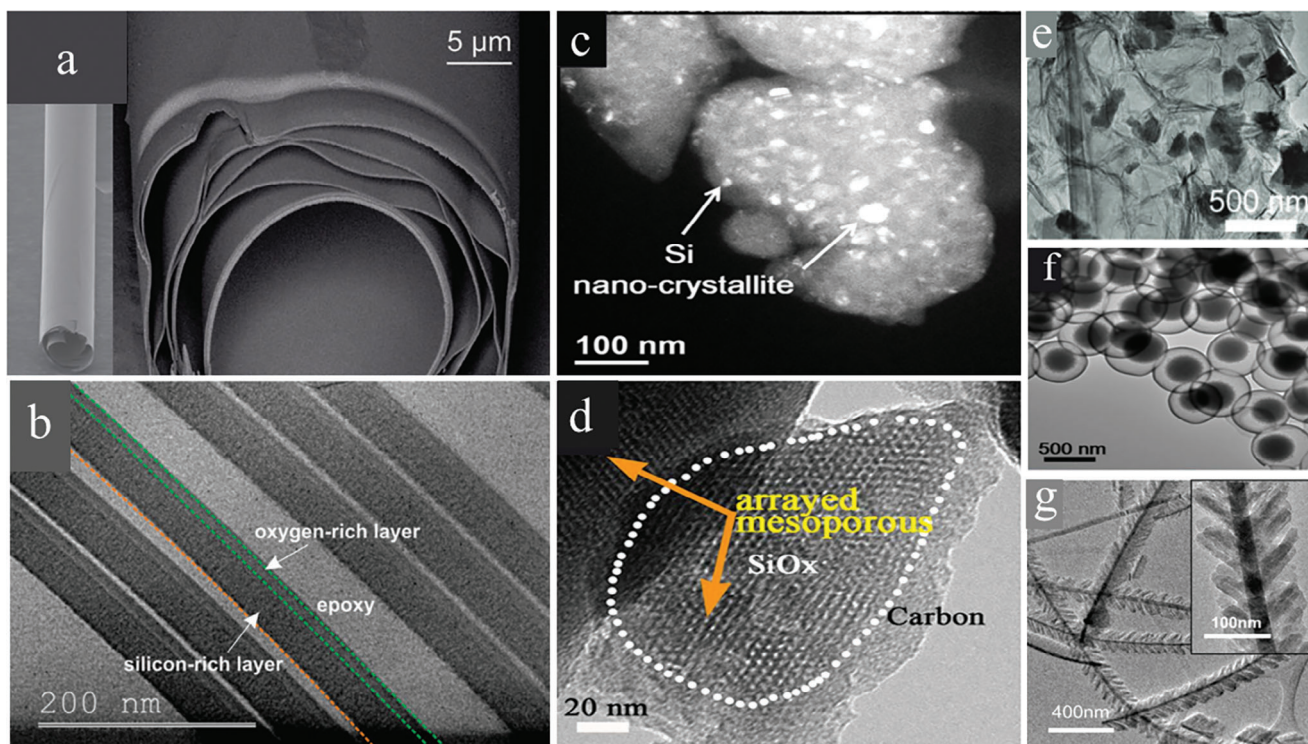


Figure 7. a,b) SEM and TEM bright-field images of rolled-up $\text{SiO}_x/\text{SiO}_y$ bilayer nanomembrane. Reprinted with permission.^[97] Copyright 2014, John Wiley and Sons. c) dark field TEM image of 10 h-HEMM $\text{Si}@\text{SiO}_x$. Reprinted with permission.^[98] Copyright 2013, Elsevier. d) TEM image of mesoporous SiO_x/C composite. Reprinted with permission.^[99] Copyright 2014, IOPscience. e) $\text{SiO}_x@\text{G}$ composite. Reprinted with permission.^[100] Copyright 2018, John Wiley and Sons. f) TEM image of SiO_x/C -CVD. Reprinted with permission.^[101] Copyright 2018, Elsevier. g) TEM image of $\text{SiO}_x/\text{NiSi}_3$ nanowires. Reprinted with permission.^[102] Copyright 2012, Elsevier.

ascribed to the highly porous structure of the composite. Nevertheless, a low ICE of 44% was observed, which can be attributed to the large specific surface area of the composite. Ma et al.^[95] utilized acid hydrolysis to extract sugar residues from RHs biomass. After a two-stage carbonization process followed by 12 h of ball-milling, the prepared C/SiO_2 composite was used as active material in anode and initially delivered a discharged capacity of 1185 mAhg^{-1} at 0.1 Ag^{-1} and an ICE of 56%. Given the simplicity and environment-friendliness of the preparation procedure, the same strategy could be used for large-scale biomass treatment. However, improvements need to be made to ICE.

2.3. Nonstoichiometric Silicon Suboxides (SiO_x)

For next-generation LIBs, nonstoichiometric silicon suboxides (SiO_x) have also been considered as attractive anode materials. Particularly, it has been found that Si-rich silicon suboxides (SiO_x , where $x < 1$) can also act as high-capacity anodes in LIBs, although they demonstrated an inferior cyclic performance. The opposite trend applies for O-rich silicon suboxides (i.e., low-capacity but praiseworthy cyclic performance).^[96] Yan et al.^[97] incorporated these two variant of silicon suboxides into a rolled-up bi-layer nano-sheets (Figure 7a,b). In 100 cycles of battery testing, the proposed bilayer nano-sheets provided a specific capacity of $\approx 1300 \text{ mAhg}^{-1}$ at 0.1 Ag^{-1} . This remarkable performance – both

in terms of capacity and durability – was attributed to the high Li storage of Si-rich sheet as well as the volume buffering effect of O-rich sheet.

Sohn et al.^[98] fabricated nanosized Si embedded in a SiO_x matrix (Figure 7c) by using high-energy mechanical milling (HEMM) and disproportionation reaction of SiO . Their study indicated good lithium storage capabilities though microstructure engineering of SiO , such that 10 h HEMM treatment of SiO delivered a reversible capacity of $\approx 1000 \text{ mAhg}^{-1}$ with low capacity retention throughout 50 cycles.

In terms of cyclability and rate capability, SiO_x/C composites have been demonstrated to outperform SiO_x without special modifications, which is basically a result of carbon's superb electrical conductivity and ability to buffer volume variations. Zhao et al.^[99] fabricated an arrayed meso-porous structure of SiO_x/C composite (Figure 7d) with an oxygen level of $x = 1.2$. The designed composite delivered a capacity of 780 mAhg^{-1} after 350 cycles at 0.1 Ag^{-1} and 0.02% decay per cycle. Xu et al.^[100] reconstructed a $\text{SiO}_x@\text{G}$ composite (Figure 7e) by encapsulating SiO_x NPs into a self-assembled graphene bubble sheet. After 1000 cycle under a current density of 1 Ag^{-1} , the synthesized $\text{SiO}_x@\text{G}$ exhibited a capacity of 780 mAhg^{-1} which is 80% of its original capacity. Using sol-gel process, selective etching, and CVD, Liu et al.^[101] coated semi-graphitic carbon on the interior and exterior surfaces of SiO_x to get a yolk@shell like SiO_x/C structure (Figure 7f). The designed nanostructure exhibited a capacity of 972 mAhg^{-1} after 500 cycles at 1 Ag^{-1} . Using LiCoO_2 as cathode

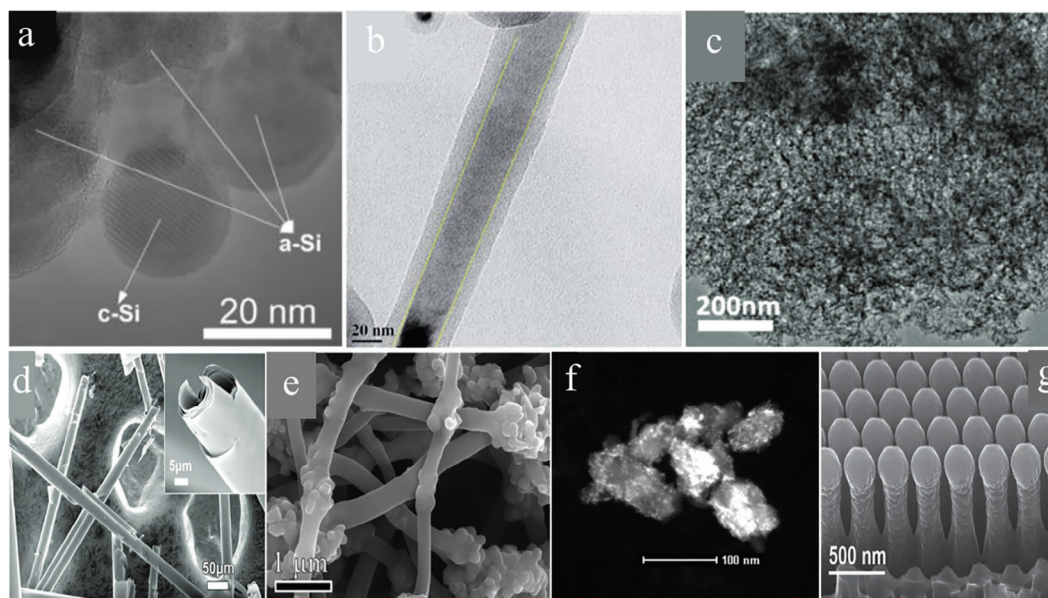


Figure 8. a) High-resolution TEM image of as-prepared Si nanoparticles. Reprinted with permission.^[124] Copyright 2016, John Wiley and Sons. b) TEM image of a-Si shell/ c-Si core nanowires. Reprinted with permission.^[125] Copyright 2018, Royal Society of Chemistry. c) TEM image of the prepared a-Si. Reprinted with permission.^[126] Copyright 2018, Royal Society of Chemistry. d) SEM image of rolled-up a-Si. Reprinted with permission.^[127] Copyright 2018, John Wiley and Sons. e) fabricated bamboo-rattle-like structure of Si/C. Reprinted with permission.^[118] Copyright 2017, John Wiley and Sons. f) dark-field SEM image of Sn coated a-Si. Reprinted with permission.^[128] Copyright 2016, Elsevier. g) SEM image of the Si/TiN/Ti/Ge nanorods. Reprinted with permission.^[129] Copyright 2015, John Wiley and Sons.

for this anode, an outstanding energy density of 428 Wh kg⁻¹ was reported.

In a similar manner to the use of metals along with SiO and SiO₂, SiO_x has also been combined with metals to improve performance and cyclability. For instance, Jo and coworkers^[102] used SiH₄ CVD and thermal evaporation to grow SiO_x/NiSi_x nanowires (Figure 7g). The synthesized nanowires exhibited a remarkable initial discharge capacity of 4058 mAhg⁻¹ at 0.15 Ag⁻¹ with an ICE of 43%, and eventually reaching to 800 mAhg⁻¹ after 100 cycles.

Table 2 provides further remarks on the electrochemical performance of Si-based anodes used in LIBs.

3. Silicon in Sodium-Ion Batteries

Similar to LIBs, it has been demonstrated that alloy-type materials possess the highest specific capacity to be used as anode in high-energy SIBs.^[114–116] The highest capacity among alloy-type materials for SIBs anodes belongs to phosphorus that forms an alloying binary phase of Na₃P offering an amazing theoretical specific capacity of 2560 mAhg⁻¹. Nevertheless, its low electrical conductivity ($\approx 10^{-14}$ S cm⁻¹), high volume expansion (>300%), and some serious safety concerns make them difficult to be integrated into real-life batteries.^[115–117] Meanwhile, Si offers a capacity of 954 mAhg⁻¹ with a volume expansion of only 114% while used in SIBs in a binary phase of NaSi, which counts for the lowest volume expansion of all alloying-type SIBs anodes.^[118–120] In light of such unique properties, Si is a very promising candidate for next-generation SIBs, and it is therefore imperative to conduct further investigative research into its application. Upon review of Si's integration in LIBs anodes, it is evident that previous

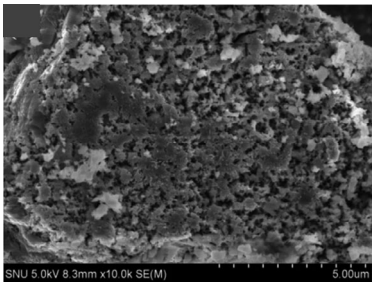
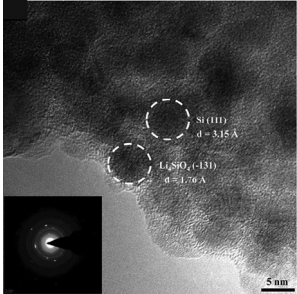
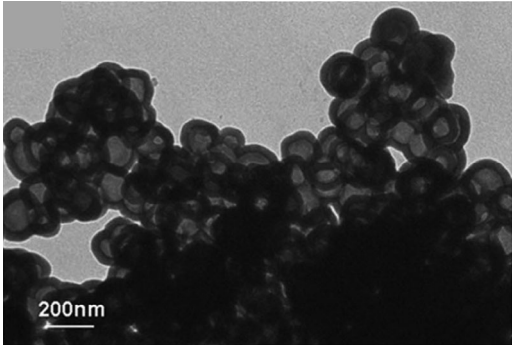
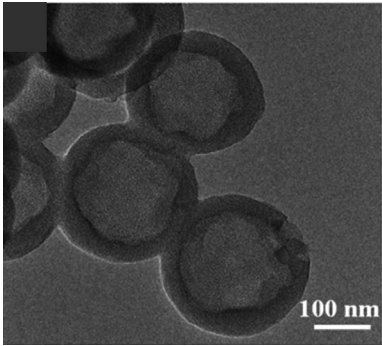
research provides valuable insight into the design of Si-based anodes, along with strategies to overcome their disadvantages (i.e., limited electrical conductivity). With a few minor adjustments, we believe that these principles could also be applied in designing Si-based anodes for SIBs.

As a first point, it is noteworthy to know that first principles calculations have demonstrated that crystalline Si (c-Si) is electrochemically inactive with elemental Na due to c-Si's high energy barrier of sodiation.^[121,122] In contrast, amorphous Si (a-Si) possesses a much lower energy barrier compared to c-Si,^[123] and hence, it has been the subject of a few research studies. For instance, Xu et al.^[124] studied reversible Na-ion uptake of Si-NPs consist of both c-Si and a-Si (Figure 8a). When cycled at 0.02 Ag⁻¹, the prepared SIB maintained a reversible capacity of 248 mAhg⁻¹ after 100 cycles. More recently, Jangid et al.^[125] fabricated Si nanowires (Figure 8b) consist of core and shell made of c-Si and a-Si, respectively, capable of delivering 125 mAhg⁻¹ after 100 cycles at a current of C/10.

A few studies have attempted to develop buffering structures for SIBs anodes. For instance, Han et al.^[126] prepared a sponge-like a-Si (Figure 8c) by reacting magnesium powder with silicon tetrachloride. Applied as an anode SIBs at 0.1 Ag⁻¹, the prepared anode could obtain a reversible capacity of 176 mAhg⁻¹ after 100 cycles. Huang et al.^[127] achieved a capacity of 152 mAhg⁻¹ at 0.5 Ag⁻¹ after a long cycling of up to 2000 cycles with an 85% capacity retention for their rolled-up a-Si nanomembranes (Figure 8d).

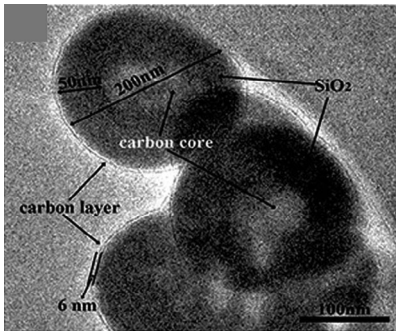
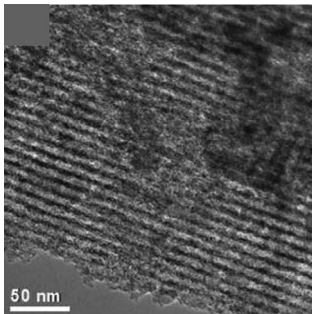
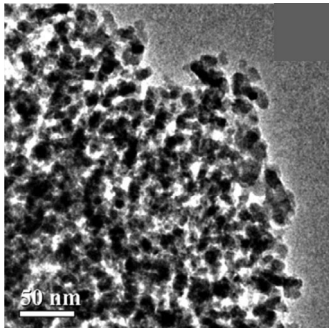
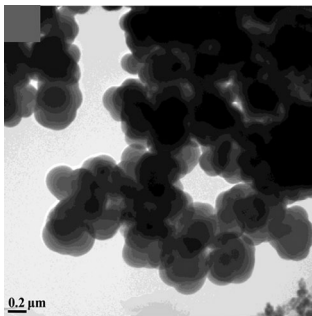
Instead of bare a-Si, some studies have used Si oxides in their preparation method. Zhang et al.^[118] utilized a combination of electrospinning, carbonization, and HF treatment to fabricate a bamboo-rattle-like structure consist of yolk-shell C/Si

Table 2. Electrochemical performance of some of Si-based anodes used in LIBs.

Composite – Reference	Composite microscopic view	Reversible cap (mAhg ⁻¹)/cycle num	Discharge rate/current	Cap retention (%)	ICE (%)
porous SiO _x - Image reprinted with permission. ^[103] Copyright 2014, Elsevier.		1242/100	0.1 C for 1 st cycle & 0.2 C for following cycles	46.8	64.4
Li/SiO - Image reprinted with permission. ^[104] Copyright 2016, Elsevier.		750/15	0.02 C	61.4	82.12
Hollow Porous SiO ₂ -nanocubes Image reprinted under terms of the CC-BY license. ^[92] Copyright 2013, Springer Nature.		919/30	0.1 Ag ⁻¹	29.7	47
hollow SiO ₂ /C nanospheres - Image reprinted with permission. ^[105] Copyright 2017, Elsevier.		441/500	0.5 Ag ⁻¹	50	68

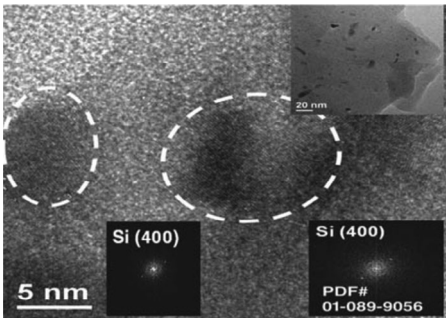
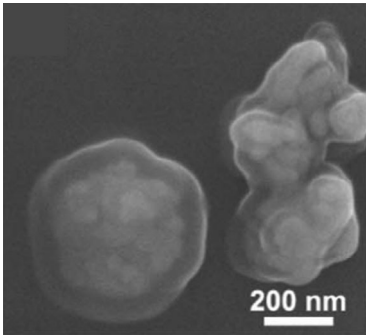
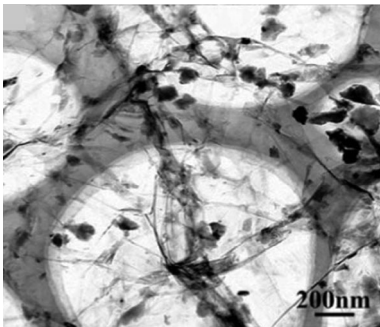
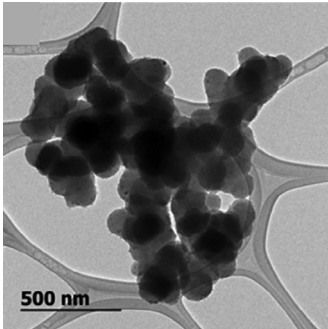
(Continued)

Table 2. Continued.

Composite – Reference	Composite microscopic view	Reversible cap (mAhg ⁻¹)/cycle num	Discharge rate/current	Cap retention (%)	ICE (%)
C/SiO ₂ /C - Image reprinted under terms of the CC-BY license. ^[106] Copyright 2015, Royal Society of Chemistry.		1055/150	0.5 Ag ⁻¹	41.4	56.5
SiO ₂ /C-N - Image reprinted with permission. ^[107] Copyright 2015, Royal Society of Chemistry.		800/100	0.2 Ag ⁻¹	27.5	42
porous SiO ₂ /C - Image reprinted with permission. ^[108] Copyright 2014, Elsevier.		210/30	1 Ag ⁻¹	78.6	59
SiO ₂ nanospheres - Image reprinted with permission. ^[109] Copyright 2014, American Chemical Society.		876.7/500	1 C	50.8	54.8

(Continued)

Table 2. Continued.

Composite – Reference	Composite microscopic view	Reversible cap (mAhg ⁻¹)/cycle num	Discharge rate/current	Cap retention (%)	ICE (%)
SiO ₂ - Image reprinted with permission. ^[110] Copyright 2012, Royal Society of Chemistry.		800/200	0.1 Ag ⁻¹	35.6	37
FeSi@Si/SiO _x - Image reprinted with permission. ^[111] Copyright 2017, Elsevier.		727/600	0.2 Ag ⁻¹	46.9	51.8
3D SiO _x /C@RGO - Image reprinted with permission. ^[112] Copyright 2014, Royal Society of Chemistry.		1284/100	0.1 Ag ⁻¹	53.4	51
Si/SiO _x /C - Image reprinted with permission. ^[113] Copyright 2014, American Chemical Society.		740/100	0.2 Ag ⁻¹	45.4	58.4

nanobeads embedded in carbon nanofibers (Figure 8e). The synthesized composite retained a reversible capacity of 454 mAhg^{-1} at 0.05 Ag^{-1} after 200 cycles. Using ether-based electrolyte, Chandra et al.^[130] successfully increased the capacity of silicon oxycarbide (SiOC) anode up to 287 mAhg^{-1} at 0.025 Ag^{-1} current density.

A number of studies have focused on the combination of a-Si with other alloying metals. A good example would be Lim et al.^[128] where they fabricated Sn coated a-Si composite (Figure 8f) capable of delivering 140 mAhg^{-1} of capacity at C/20 and after 5 cycles. Also, Yue et al.^[129] fabricated hexagonal match-like Si/Ge nanorods buffered by TiN/Ti interlayering medium (Figure 8g) via a cost-effective approach. After 200 cycles at 0.4 Ag^{-1} , a reversible capacity of 390 mAhg^{-1} and an ICE of 50% was recorded for their composite.

As can be seen, there has been a relatively small amount of research conducted on Si-based anodes for SIBs. There are several reasons for this disparity in research:

Maturity of technologies: Since the 1990s, LIBs have been commercially available and are now the dominant energy storage technology for portable electronics, electric vehicles, and a wide variety of other applications.^[131] Considering this, LIBs have received a great deal of attention with regards to improving their performance, which has led to research into materials like Si that can enhance battery performance. Compared to LIBs however, SIBs are relatively newer and have not reached the same level of maturity or commercial scale. Therefore, SIB research is still in its infancy, and the exploration of advanced anode materials such as Si is limited.

Electrochemical behavior of Si in SIBs: As a result of Si alloying with lithium, Si-based anodes in LIBs have contributed to a high theoretical specific capacity. In contrast to LIBs, Si's alloying reaction with sodium is not as favorable, and as discussed before, is almost limited to a-Si.^[123] Researchers may be discouraged from conducting research due to this reduced benefit.

Initial focus of SIBs: One of the main motivations behind the development of SIBs is to create a more cost-effective alternative to LIBs by leveraging the abundance and availability of sodium.^[132] Initial research, as well as more current research trend on SIBs has therefore been more focused on using abundant, cheap, and easily accessible materials like layered oxide cathodes.^[133–137]

Research funding and commercial interests: The success of LIBs and their widespread adoption has resulted in substantial funding for research to improve their performance. Because SIBs are still emerging and do not have the commercial success of conventional LIBs,^[138,139] there may be fewer resources allocated to advanced materials research for SIBs, including the exploration of Si-based anodes.

Infrastructure and expertise: Research infrastructure, expertise, and focus have been heavily geared toward LIBs due to their commercial importance. The momentum created by the LIB technology can naturally lead to continued exploration of materials like Si-NPs, whereas newer technologies like SIBs might require longer to gain traction.

Although the current disparity between Si research in LIBs and SIBs may be explained by these reasons, but it is also important to note that as SIB technology matures and becomes more commercially relevant, there will be a greater interest in exploring ad-

vanced anode materials, including Si, that can improve SIB performance.

Given the burgeoning interest in harnessing the potential of Si-based anodes for SIBs, and considering the examination of Si-based anodes in LIBs, we identify the following critical aspects that need be considered to increase the actual sodium storage capacity of Si-NPs anodes and help their scaling up process.

3.1. Volume Fluctuations

The anode's volume expansion leads to particle fragmentation, which prompts the reformation of SEI layer. Consequently, the availability of Na^+ ions for the alloying process diminishes, reducing the overall capacity. Using hollow porous structures can enhance the anode's resilience to mechanical stresses during sodiation/desodiation. During sodiation, hollow structures can provide space to accommodate silicon's volume expansion. During the expansion process of silicon, the void space within the hollow structure acts as a buffer, preventing or reducing the possibility of particle fracture and preserving the structural integrity of the anode. Nevertheless, it is important to note that there are both advantages and disadvantages associated with hollow structures in terms of energy density. On the positive side hollow structures can maintain better electrical connectivity and thus better energy delivery over numerous charge/discharge cycles by preventing extensive particle fracture. On the other hand, however, the existence of void spaces might also result in a decrease in active material content per unit volume, potentially reducing the overall energy storage capacity. Therefore, a trade-off between mechanical stability and energy density would need to be carefully balanced while considering hollow structures.

Another strategy in mitigating the effects of volume expansion involves integrating Si-NPs into a flexible carbonaceous matrix. Using carbonaceous matrix as the scaffold to Si-NPs can also act as a protective coating which minimizes direct exposure to the electrolyte, reducing undesirable SEI formation. Given the superior Na storage capabilities of hard carbon,^[33,140–143] incorporating Si-NPs within such a medium can be particularly more advantageous. The use of hard carbon as an anode for SIBs is becoming more popular, but until the writing of this review, hard carbon has not been used for accommodating Si-NPs. The restrained advancement of Si-NPs in hard carbon anodes can be attributed to several factors, including conductivity mismatch, compatibility with electrolyte, incomplete comprehension of Na storage in hard carbon, challenges in production, as well as concerns regarding cost and scalability, among others.

Using Si-NPs in their suboxides form as an alternative to pure Si-NPs can also offer several advantages, including smaller volume expansion. As previously discussed in LIBs, Si suboxides exhibit smaller volume expansion compared to their pure Si counterparts, minimizing mechanical stress, and enhancing anode durability. The cost-effective nature of Si suboxides can make the production and scaling of SIBs more financially viable, thereby potentially accelerating their adoption in various applications. While using Si suboxides comes with the drawback of a reduced theoretical capacity, it is possible to modulate the oxygen content of these compounds through various reduction methods. Such fine-tuning offers a balanced trade-off between anode's volume

expansion and theoretical capacity, paving the way for optimized its performance.

3.2. Electrolyte Compatibility

Side reactions between the electrolyte and Si contribute to non-ideal SEI formation and effectively reducing overall sodium storage capacity of the anode.^[144] Investigating and utilizing electrolytes with specific additives that remain stable across both low and high potentials can help curb such side reactions and foster the creation of a stable, thin SEI layer. In a general sense, for SIBs to achieve high capacity, stability, and flexibility, the electrolyte should possess these essential attributes:^[145–147]

- Ionic conductivity exceeding 0.1 mS cm^{-1} at room temperature and higher,
- High Na^+ transference number with minimal electronic transference,
- Wide electrochemical stability range,
- Robust mechanical and thermal resilience,
- Long-lasting durability, ensuring sustained performance under the specific device's operational conditions,
- Environmental considerations, and
- Cost-efficiency.

Furthermore, development of durable solid-state electrolytes presents additional advantages, including mitigating safety concerns with some conventional liquid electrolytes.^[148]

3.3. Sodium Related kinetic Limitations

The larger ionic size of Na^+ compared to Li^+ can result in slower diffusion rates within anode structure.^[22] Designing engineered Si structures with larger specific surface area, such as porous Si, Si nanowires, nanotubes, or hollow spheres can shorten the diffusion pathways for Na^+ ions, thus enhancing the kinetics of sodium insertion and extraction.

3.4. Incomplete Alloying

Under typical battery operation conditions, the conversion to NaSi might not be complete, resulting in incomplete alloying and a consequent reduction in capacity. Similar to LIBs, enhancing the degree of alloying in SIBs can be achieved by optimizing electrode fabrication and using binders that are compatible with alloying/dealloying processes.^[138,149]

3.5. Silicon from Biomass-Based Materials

One of the primary motivations behind developing SIBs is to produce a cost-effective energy storage solution. Given this trend, introducing high-cost materials (like certain forms of Si nanocomposites) into SIBs might run counter to the primary motivation of cost savings in some cases. A promising approach to reducing Si production costs is to use biomass as a precursor to produce Si-based materials. Biomass-derived Si, depending on the

processing route and the source of the biomass, can potentially produce a high yield of Si. Rice husks are good example for having high silica content which has already been used as a suitable Si precursor in LIBs.^[93–95]

For biomass-derived Si, the typical process involves initial acid washing to remove the impurities. This is usually followed by a reduction process to convert the silica to silicon. Depending on the preparation procedure, the resulting silicon might be in the form of amorphous silicon (a-Si) or nanoparticles (Si-NPs), integrated within a carbonaceous matrix.^[95] Given that this Si is derived from a low-cost, abundant source, it is fully aligned with the cost-saving motivations of SIBs development.

3.6. Silicon-Based Alloys and Heteroatom Doping

By alloying Si with metals that have higher electrical conductivity, the electrochemical stability can be improved. This can potentially lead to a more consistent and prolonged charge/discharge cycling performance, reducing the rapid capacity fade observed with pure Si. Examples of such Hybrid nanocomposites are porous Si/silver nanostructures used in high-performance photovoltaic devices,^[150] SiO_2/Ni nanocomposite used in LIBs anodes,^[87] and Si/Ge nanorods in SIBs anodes.^[129] Furthermore, heteroatom doping has been used as an approach to increase the electrical conductivity of the anode composites, as well as tuning the interlayer spacing of hard carbon.^[28,151–154] Such alloys and doping strategies can be further studied and utilized for high-performance Si-based anodes.

4. Conclusion

While Si boasts the highest theoretical capacity and exhibits the least volume expansion among alloying-type Sodium-ion batteries (SIBs) anode compounds, it remains an underexplored area in the development of high-performance SIBs. Reflecting on Si's storied past in Lithium-ion batteries (LIBs), the transformative role of nanoengineering becomes evident. By creating nanostructured alloys, benefits such as increased gravimetric capacities, enhanced fracture resistance, shorter ionic diffusion paths, and controlled volume expansion are realized. Through this review, we encapsulated the evolution and adaptations of Si-NPs in LIBs, to provide valuable insights for their prospective application in emerging battery technologies, especially SIBs. On a broader scale, it's evident that Si-based anodes in SIBs are still in their nascent stages of research. Drawing from our comprehensive literature survey, we identify the following aspects that require attention in future research path toward high-performing Si-based anodes in SIBs:

Anode volume expansion leads to particle pulverization, which contributes to battery cycle life shortening. While the volume swelling of Si in SIBs anodes is relatively smaller than that of LIBs (400% in LIBs vs. only 114% in SIBs), it must still be addressed for commercializing SIBs.

Similar to the existing studies in LIBs, hollow structures can be developed and used as an approach in alleviating the volume expansion of Si-based SIBs anodes. However, it is important to carefully maintain a balance between energy density and mechanical stability while considering hollow structures.

Si-NPs integrated into graphitic carbon matrix, which is a popular method for alleviating Si-NPs volume expansion effects in LIBs, might not be equally effective in SIBs. The reason for this is primarily due to the larger ionic radius of Na compared to Li, which limits its intercalation into graphite layers. Hard carbon, on the other hand, has a larger interlayer spacing and is therefore a more suitable host for Si-NPs in SIBs. In this manner, a composite of Si-NPs inside a matrix of hard carbon can provide a more reliable anode for SIBs.

Although hard carbon is becoming a popular anode for SIBs, it has not been explored for the integration of Si-NPs. However, integrating Si-NPs into hard carbon anodes for SIBs remains a highly promising prospect, especially when considering emerging strategies and technological developments. The use of biomass-derived hard carbon that naturally contains Si is an eco-friendly and potentially cost-effective method, taking advantage of the inherent properties of both materials. Furthermore, advanced material engineering approaches offer tailor-made solutions that can overcome existing challenges. The manipulation of the structural composition and optimization of the nano-architecture, for example, may provide a solution to the issues of compatibility and conductivity. Moreover, the exploration of novel binders, surface treatments, and hybrid structures may facilitate a more harmonious integration of Si into hard carbon anodes.

Heteroatom doping has already been extensively used in improving the electrical conductivity of Si-based LIBs anodes. The same strategy needs to be studied further in SIBs as well.

Nanoscale Si could be considered an expensive anode active material due to the high cost of production. For applications requiring a high level of cost savings and sustainability, using Si-rich biomass is highly recommended. Si-NPs are naturally integrated within a carbon matrix inside these biomass precursors in form of SiO_x. A variety of structural formations with desirable properties can be produced by optimizing the preparation conditions, such as carbonization temperature, heat rate, atmospheric gas composition, heteroatom additives, to name a few.

To achieve high energy efficiency, it is imperative to optimize the oxygen content of Si oxides active materials. In general, higher levels of oxygen are necessary for battery applications with a long lifespan, while lower levels of oxygen are needed for high-capacity battery applications. This calls for more experimental studies on the use of different controllable reduction methods for Si-based anodes in SIBs.

The use of Si in conjunction with metallic elements can also facilitate the development of high-performance SIBs. As a result, there are many potential avenues for exploration in this area.

Na storage in hard carbon as well as the mechanism of reaction between Na and Si oxides are still subjects of discussion. Gaining an in-depth understanding of these mechanisms is necessary for designing better Si oxide-based anodes.

Acknowledgements

This work was supported by UEA's Critical Decade for Climate Change Doctoral Training Program, funded by the Leverhulme Trust under their Doctoral Scholarship Scheme.

Conflict of Interest

The authors declare no conflict of interest.

Keywords

anode materials, lithium-ion batteries, silicon nanoparticles, sodium-ion batteries

Received: August 22, 2023

Revised: October 25, 2023

Published online:

- [1] F. J. de Sisternes, J. D. Jenkins, A. Botterud, *Appl. Energy* **2016**, *175*, 368.
- [2] M. Arbabzadeh, R. Sioshansi, J. X. Johnson, G. A. Keoleian, *Nat. Commun.* **2019**, *10*, 3413.
- [3] L. Zu, W. Zhang, L. Qu, L. Liu, W. Li, A. Yu, D. Zhao, *Adv. Energy Mater.* **2020**, *10*, 38.
- [4] N. A. Sepulveda, J. D. Jenkins, A. Edington, D. S. Mallapragada, R. K. Lester, *Nat. Energy* **2021**, *6*, 506.
- [5] G. Li, S. Guo, B. Xiang, S. Mei, Y. Zheng, X. Zhang, B. Gao, P. K. Chu, K. Huo, *Energy Mater.* **2022**, *2*, 200020.
- [6] L. Zhai, G. Li, X. Yang, S. Park, D. Han, L. Mi, Y. Wang, Z. Li, S. Y. Lee, *Adv. Funct. Mater.* **2022**, *32*, 9.
- [7] K. Mishra, N. Yadav, S. A. Hashmi, *J. Mater. Chem. A Mater.* **2020**, *8*, 22507.
- [8] J. U. Choi, N. Voronina, Y. K. Sun, S. T. Myung, *Adv. Energy Mater.* **2020**, *10*, 42.
- [9] X. Pu, H. Wang, D. Zhao, H. Yang, X. Ai, S. Cao, Z. Chen, Y. Cao, *Small* **2019**, *15*, 32.
- [10] B. Xiao, T. Rojo, X. Li, *ChemSusChem* **2019**, *12*, 133.
- [11] T. Perveen, M. Siddiq, N. Shahzad, R. Ihsan, A. Ahmad, M. I. Shahzad, *Renew. Sustain. Ener. Rev.* **2020**, *119*, 109549.
- [12] S. Liang, Y. J. Cheng, J. Zhu, Y. Xia, P. Müller-Buschbaum, *Small Methods* **2020**, *4*, 8.
- [13] H. Tan, D. Chen, X. Rui, Y. Yu, *Adv. Funct. Mater.* **2019**, *29*, 14.
- [14] L. Wang, J. Światowska, S. Dai, M. Cao, Z. Zhong, Y. Shen, M. Wang, *Mater Today Energy* **2019**, *11*, 46.
- [15] H. Zhang, I. Hasa, S. Passerini, *Adv. Energy Mater.* **2018**, *8*, 17.
- [16] C. Wu, S. X. Dou, Y. Yu, *Small* **2018**, *14*, 22.
- [17] Y. Lu, L. Yu, X. W. (David) Lou, *Chem* **2018**, *4*, 972.
- [18] X. Li, Y. Wang, L. Lv, G. Zhu, Q. Qu, H. Zheng, *Energy Materials* **2022**, *2*, 200014.
- [19] P. C. Tsai, S. C. Chung, S. K. Lin, A. Yamada, *J Mater Chem A Mater* **2015**, *3*, 9763.
- [20] P. Ge, M. Foulletier, *Solid State Ion* **1988**, *28*, 1172.
- [21] P. C. Tsai, S. C. Chung, S. K. Lin, A. Yamada, *J. Mater. Chem. A Mater.* **2015**, *3*, 9763.
- [22] L. F. Zhao, Z. Hu, W. H. Lai, Y. Tao, J. Peng, Z. C. Miao, Y. X. Wang, S. L. Chou, H. K. Liu, S. X. Dou, *Adv. Energy Mater.* **2021**, *11*, 1.
- [23] J. Zhang, D.-W. Wang, W. Lv, L. Qin, S. Niu, S. Zhang, T. Cao, F. Kang, Q.-H. Yang, *Adv. Energy Mater.* **2018**, *8*, 1801361.
- [24] G. Li, K. Chen, Y. Wang, Z. Wang, X. Chen, S. Cui, Z. Wu, C. Soutis, W. Chen, L. Mi, *Nanoscale* **2020**, *12*, 8493.
- [25] Y. Kim, J.-K. Kim, C. Vaalma, G. H. Bae, G.-T. Kim, S. Passerini, Y. Kim, *Carbon N Y* **2018**, *129*, 564.
- [26] M. Saavedra, L. Simonin, C. Matei, C. Vaultot, S. Perez, C. Dupont, *Fuel Process. Technol.* **2021**, *231*, 107223.
- [27] Y. Li, S. Xu, X. Wu, J. Yu, Y. Wang, Y.-S. Hu, H. Li, L. Chen, X. Huang, *J. Mater. Chem. A Mater.* **2015**, *3*, 71.
- [28] F. Wu, L. Liu, Y. Yuan, Y. Li, Y. Bai, T. Li, J. Lu, C. Wu, *ACS Appl. Mater. Interfaces* **2018**, *10*, 27030.
- [29] D. Chen, W. Zhang, K. Luo, Y. Song, Y. Zhong, Y. Liu, G. Wang, B. Zhong, Z. Wu, X. Guo, *Energy Environ. Sci.* **2021**, *14*, 2244.

- [30] Y. Sun, H. Wang, Z. Qu, K. Wang, L. Wang, J. Gao, J. Gao, S. Liu, F. Lu, *Adv. Energy Mater.* **2021**, *11*, 2002981.
- [31] C. Wu, M. Zhang, Y. Bai, X. Wang, R. Dong, F. Wu, *ACS Appl. Mater. Interfaces* **2019**, *11*, 12554.
- [32] T.-P. Mehmood, G. Ali, B. Koyutuerk, J. Pampel, K. Y. Chung, A. Fellingner, *Energy Storage Mater.* **2020**, *28*, 101.
- [33] B. Sun, Z. Guan, Y. Liu, Y. Cao, Q. Zhu, H. Liu, Z. Wang, P. Zhang, N. Xu, *Adv. Energy Mater.* **2019**, *9*, 1901351.
- [34] J. Xiao, H. Lu, Y. Fang, M. L. Sushko, Y. Cao, X. Ai, H. Yang, L. Liu, *Adv. Energy Mater.* **2018**, *8*, 1703238.
- [35] H. Hou, X. Qiu, W. Wei, Y. Zhang, X. Ji, *Adv. Energy Mater.* **2017**, *7*, 24.
- [36] H. Chang, Y.-R. Wu, X. Han, T.-F. Yi, *Energy Materials* **2022**, *1*, 100003.
- [37] K. Chen, G. Li, Z. Hu, Y. Wang, Z. Wang, N. Qin, X. Chen, W. Chen, Z. Wu, C. Soutis, L. Mi, *Energy and Fuels* **2021**, *35*, 6265.
- [38] X. Xiong, C. Yang, G. Wang, Y. Lin, X. Ou, J. H. Wang, B. Zhao, M. Liu, Z. Lin, K. Huang, *Energy Environ. Sci.* **2017**, *10*, 1757.
- [39] X. Ou, L. Cao, X. Liang, F. Zheng, H. S. Zheng, X. Yang, J. H. Wang, C. Yang, M. Liu, *ACS Nano* **2019**, *13*, 3666.
- [40] C. Yang, X. Liang, X. Ou, Q. Zhang, H. S. Zheng, F. Zheng, J. H. Wang, K. Huang, M. Liu, *Adv. Funct. Mater.* **2019**, *29*, 9.
- [41] L. Cao, X. Liang, X. Ou, X. Yang, Y. Li, C. Yang, Z. Lin, M. Liu, *Adv. Funct. Mater.* **2020**, *30*, 16.
- [42] T. L. Kulova, A. M. Skundin, *Energies (Basel)* **2022**, *15*, 22.
- [43] M. Lao, Y. Zhang, W. Luo, Q. Yan, W. Sun, S. X. Dou, *Adv. Mater.* **2017**, *29*, 48.
- [44] H. Gao, W. Ma, W. Yang, J. Wang, J. Niu, F. Luo, Z. Peng, Z. Zhang, *J. Power Sources* **2018**, *379*, 1.
- [45] J. Sottmann, M. Herrmann, P. Vajeeston, Y. Hu, A. Ruud, C. Drathen, H. Emerich, H. Fjellvåg, D. S. Wragg, *Chem. Mater.* **2016**, *28*, 2750.
- [46] D. Su, S. Dou, G. Wang, *Nano Energy* **2015**, *12*, 88.
- [47] W. Devina, H. Setiadi Cahyadi, I. Albertina, C. Chandra, J. H. Park, K. Yoon Chung, W. Chang, S. Kyu Kwak, J. Kim, *Chem. Eng. J.* **2022**, *432*.
- [48] P. Li, H. Kim, S. Myung, Y. Sun, *Energy Storage Mater.* **2021**, *35*, 550.
- [49] S. C. Jung, D. S. Jung, J. W. Choi, Y. K. Han, *J. Phys. Chem. Lett.* **2014**, *5*, 1283.
- [50] Abundance of elements in the earth's crust and in the sea, CRC Handbook of Chemistry and Physics, 2nd ed **2017**.
- [51] 'The Mineral Resources Program by USGS, Abundance of elements' **2016**.
- [52] A. R. Kamali, D. J. Fray, *New Mat. for Electrochem. Systems* **2010**, *13*, 147.
- [53] H. K. Liu, Z. P. Guo, J. Z. Wang, K. Konstantinov, *J. Mater. Chem.* **2010**, *20*, 10055.
- [54] H. Kim, E. J. Lee, Y. K. Sun, *Mater. Today* **2014**, *17*, 285.
- [55] P. Li, G. Zhao, X. Zheng, X. Xu, C. Yao, W. Sun, *Energy Storage Mater.* **2018**, *15*, 422.
- [56] L. Sun, Y. Liu, R. Shao, J. Wu, R. Jiang, Z. Jin, *Energy Storage Mater.* **2022**, *46*, 482.
- [57] C. K. Chan, H. Peng, G. Liu, K. Mclwrath, X. F. Zhang, R. A. Huggins, Y. Cui, *Nat. Nanotechnol.* **2008**, *3*, 31.
- [58] Y. Liu, L. Qin, F. Liu, Y. Fan, J. Ruan, S. Zhang, *J. Power Sources* **2018**, *406*, 167.
- [59] J. Liu, Y. Yang, P. Lyu, P. Nachtigall, Y. Xu, *Adv. Mater.* **2018**, *30*, 26.
- [60] T. Xu, D. Wang, P. Qiu, J. Zhang, Q. Wang, B. Xia, X. Xie, *Nanoscale* **2018**, *10*, 16638.
- [61] B. Wang, X. Li, B. Luo, L. Hao, M. Zhou, X. Zhang, Z. Fan, L. Zhi, *Adv. Mater.* **2015**, *27*, 1526.
- [62] C. Pang, H. Song, N. Li, C. Wang, *RSC Adv.* **2015**, *5*, 6782.
- [63] J. Ma, H. Tan, H. Liu, Y. Chao, *Particle and Particle Systems Characterization* **2021**, *38*, 2000288.
- [64] T. Zhang, C. Chen, X. Bian, B. Jin, Z. Li, H. Xu, Y. Xu, Y. Ju, *RSC Adv.* **2022**, *12*, 19678.
- [65] D. Lin, Z. Lu, P. C. Hsu, H. R. Lee, N. Liu, J. Zhao, H. Wang, C. Liu, Y. Cui, *Energy Environ. Sci.* **2015**, *8*, 2371.
- [66] C. Wang, H. Wu, Z. Chen, M. T. McDowell, Y. Cui, Z. Bao, *Nat. Chem.* **2013**, *12*, 1042.
- [67] S. W. Lee, M. T. McDowell, J. W. Choi, Y. Cui, *Nano Lett.* **2011**, *11*, 3034.
- [68] M. Pasta, C. D. Wessells, R. A. Huggins, Y. Cui, *Nat. Commun.* **2012**, *3*.
- [69] H. Kim, M. Seo, M. H. Park, J. Cho, *Angewandte Chemie – International Edition* **2010**, *49*, 2146.
- [70] M. Yamada, A. Ueda, K. Matsumoto, T. Ohzuku, *J. Electrochem. Soc.* **2011**, *158*, A417.
- [71] M. Yamada, K. Uchitomi, A. Ueda, K. Matsumoto, T. Ohzuku, *J. Power Sources* **2013**, *225*, 221.
- [72] L. Shi, C. Pang, S. Chen, M. Wang, K. Wang, Z. Tan, P. Gao, J. Ren, Y. Huang, H. Peng, Z. Liu, *Nano Lett.* **2017**, *17*, 3681.
- [73] M. Zhou, M. L. Gordin, S. Chen, T. Xu, J. Song, D. Lv, D. Wang, *Electrochem. Commun.* **2013**, *28*, 79.
- [74] B. Liu, A. Abouimrane, Y. Ren, M. Balasubramanian, D. Wang, Z. Z. Fang, K. Amine, *Chemistry of Materials* **2012**, *24*, 4653.
- [75] B. Liu, A. Abouimrane, D. E. Brown, X. Zhang, Y. Ren, Z. Z. Fang, K. Amine, *J Mater Chem A Mater* **2013**, *13*, 4376.
- [76] M. Miyachi, H. Yamamoto, H. Kawai, *J. Electrochem. Soc.* **2007**, *154*, A376.
- [77] H. Yamamura, S. Nakanishi, H. Iba, *J. Power Sources* **2013**, *232*, 264.
- [78] Y. Zhong, M. Yang, X. Zhou, Z. Zhou, *Mater. Horiz.* **2015**, *6*, 553.
- [79] P. G. Bruce, B. Scrosati, J. M. Tarascon, *Angewandte Chemie – International Edition* **2008**, *47*, 2930.
- [80] Y. Sun, N. Liu, Y. Cui, *Nat. Energy* **2016**, *1*, 7.
- [81] C. Liang, L. Zhou, C. Zhou, H. Huang, S. Liang, Y. Xia, Y. Gan, X. Tao, J. Zhang, W. Zhang, *Mater. Res. Bull.* **2017**, *96*, 347.
- [82] Z. Favors, W. Wang, H. H. Bay, A. George, M. Ozkan, C. S. Ozkan, *Sci. Rep.* **2014**, *4*.
- [83] X. Ma, Z. Wei, H. Han, X. Wang, K. Cui, L. Yang, *Chem. Eng. J.* **2017**, *323*, 252.
- [84] H. H. Li, L. L. Zhang, C. Y. Fan, K. Wang, X. L. Wu, H. Z. Sun, J. P. Zhang, *Phys. Chem. Chem. Phys.* **2015**, *17*, 22893.
- [85] X. Wu, Z. Q. Shi, C. Y. Wang, J. Jin, *J. Electroanal. Chem.* **2015**, *746*, 62.
- [86] D. Wang, T. Wang, M. He, T. Wang, H. Wang, *Nano, Macro, Small* **2021**, *17*, 2103878.
- [87] C. Tang, Y. Liu, C. Xu, J. Zhu, X. Wei, L. Zhou, L. He, W. Yang, L. Mai, *Adv. Funct. Mater.* **2018**, *28*, 3.
- [88] Y. Yao, J. Zhang, L. Xue, T. Huang, A. Yu, *J. Power Sources* **2011**, *196*, 10240.
- [89] M. Li, Y. Yu, J. Li, B. Chen, X. Wu, Y. Tian, P. Chen, *J Mater Chem A Mater* **2015**, *3*, 1476.
- [90] J. Meng, Y. Cao, Y. Suo, Y. Liu, J. Zhang, X. Zheng, *Electrochim. Acta* **2015**, *176*, 1001.
- [91] Z. Xiang, Y. Chen, J. Li, X. Xia, Y. He, H. Liu, *J. Solid State Electrochem.* **2017**, *21*, 2425.
- [92] N. Yan, F. Wang, H. Zhong, Y. Li, Y. Wang, L. Hu, Q. Chen, *Sci. Rep.* **2013**, *3*.
- [93] Y. Li, L. Liu, X. Liu, Y. Feng, L. Yu, Z. He, X. Cui, M. Zhang, Y. Zhu, *Ionics (Kiel)* **2022**, *151*.
- [94] Y. Li, L. Liu, X. Liu, Y. Feng, B. Xue, L. Yu, L. Ma, Y. Zhu, Y. Chao, X. Wang, *Mater. Chem. Phys.* **2021**, *262*, 124331.
- [95] L. Ma, L. Liu, X. Liu, Y. Li, Y. Feng, Y. Tian, Y. Chao, Y. Zhu, X. Wang, *J. Electron. Mater.* **2021**, *50*, 4426.
- [96] C. Y. Chou, G. S. Hwang, *Chem. Mater.* **2013**, *25*, 3435.
- [97] L. Zhang, J. Deng, L. Liu, W. Si, S. Oswald, L. Xi, M. Kundu, G. Ma, T. Gemming, S. Baunack, F. Ding, C. Yan, O. G. Schmidt, *Adv. Mater.* **2014**, *26*, 4527.
- [98] Y. Hwa, C. M. Park, H. J. Sohn, *J. Power Sources* **2013**, *222*, 129.

- [99] C. Gao, H. Zhao, P. Lv, C. Wang, J. Wang, T. Zhang, Q. Xia, *J. Electrochem. Soc.* **2014**, *161*, A2216.
- [100] Q. Xu, J. K. Sun, Z. L. Yu, Y. X. Yin, S. Xin, S. H. Yu, Y. G. Guo, *Adv. Mater.* **2018**, *30*, 25.
- [101] Z. Liu, Y. Zhao, R. He, W. Luo, J. Meng, Q. Yu, D. Zhao, L. Zhou, L. Mai, *Energy Storage Mater.* **2019**, *19*, 299.
- [102] K. Song, S. Yoo, K. Kang, H. Heo, Y. M. Kang, M. H. Jo, *J. Power Sources* **2013**, *229*, 229.
- [103] B. C. Yu, Y. Hwa, J. H. Kim, H. J. Sohn, *Electrochim. Acta* **2014**, *117*, 426.
- [104] J. H. Yom, S. W. Hwang, S. M. Cho, W. Y. Yoon, *J. Power Sources* **2016**, *311*, 159.
- [105] W. An, J. Fu, J. Su, L. Wang, X. Peng, K. Wu, Q. Chen, Y. Bi, B. Gao, X. Zhang, *J. Power Sources* **2017**, *345*, 227.
- [106] X. Cao, X. Chuan, R. C. Massé, D. Huang, S. Li, G. Cao, *J. Mater. Chem. A Mater.* **2015**, *3*, 22739.
- [107] Y. Liang, L. Cai, L. Chen, X. Lin, R. Fu, M. Zhang, D. Wu, *Nanoscale* **2015**, *7*, 3971.
- [108] X. Yang, H. Huang, Z. Li, M. Zhong, G. Zhang, D. Wu, *Carbon N Y* **2014**, *77*, 275.
- [109] J. Tu, Y. Yuan, P. Zhan, H. Jiao, X. Wang, H. Zhu, S. Jiao, *J. Phys. Chem. C* **2014**, *118*, 7357.
- [110] W. S. Chang, C. M. Park, J. H. Kim, Y. U. Kim, G. Jeong, H. J. Sohn, *Energy Environ. Sci.* **2012**, *5*, 6895.
- [111] W. He, Y. Liang, H. Tian, S. Zhang, Z. Meng, W. Q. Han, *Energy Storage Mater.* **2017**, *8*, 119.
- [112] C. Guo, D. Wang, T. Liu, J. Zhu, X. Lang, *J. Mater. Chem. A Mater* **2014**, *2*, 3521.
- [113] M. S. Park, E. Park, J. Lee, G. Jeong, K. J. Kim, J. H. Kim, Y. J. Kim, H. Kim, *ACS Appl. Mater. Interfaces* **2014**, *6*, 9608.
- [114] J. Qian, Y. Chen, L. Wu, Y. Cao, X. Ai, H. Yang, *Chem. Commun.* **2012**, *48*, 7070.
- [115] W. Li, S. L. Chou, J. Z. Wang, J. H. Kim, H. K. Liu, S. X. Dou, *Adv. Mater.* **2014**, *26*, 4037.
- [116] C. Chen, K. Fu, Y. Lu, J. Zhu, L. Xue, Y. Hu, X. Zhang, *RSC Adv.* **2015**, *5*, 30793.
- [117] Y. Kim, Y. Park, A. Choi, N. S. Choi, J. Kim, J. Lee, J. H. Ryu, S. M. Oh, K. T. Lee, *Adv. Mater.* **2013**, *25*, 3045.
- [118] L. Zhang, X. Hu, C. Chen, H. Guo, X. Liu, G. Xu, H. Zhong, S. Cheng, P. Wu, J. Meng, Y. Huang, S. Dou, H. Liu, *Adv. Mater.* **2017**, *29*, 5.
- [119] D. H. Nam, T. H. Kim, K. S. Hong, H. S. Kwon, *ACS Nano* **2014**, *8*, 11824.
- [120] S. C. Jung, H. J. Kim, Y. J. Kang, Y. K. Han, *J. Alloys Compd.* **2016**, *688*, 158.
- [121] V. V. Kulish, O. I. Malyi, M. F. Ng, Z. Chen, S. Manzhos, P. Wu, *Phys. Chem. Chem. Phys.* **2014**, *16*, 4260.
- [122] S. M. Zheng, Y. R. Tian, Y. X. Liu, S. Wang, C. Q. Hu, B. Wang, K. M. Wang, *Rare Met.* **2021**, *40*, 272.
- [123] M. K. Jangid, A. Vemulapally, F. J. Sonia, M. Aslam, A. Mukhopadhyay, *J. Electrochem. Soc.* **2017**, *164*, A2559.
- [124] Y. Xu, E. Swaans, S. Basak, H. W. Zandbergen, D. M. Borsa, F. M. Mulder, *Adv. Energy Mater.* **2016**, *6*, 2.
- [125] M. K. Jangid, A. S. Lakhnot, A. Vemulapally, F. J. Sonia, S. Sinha, R. O. Dusane, A. Mukhopadhyay, *J. Mater. Chem. A Mater* **2018**, *6*, 3422.
- [126] Y. Han, N. Lin, T. Xu, T. Li, J. Tian, Y. Zhu, Y. Qian, *Nanoscale* **2018**, *10*, 3153.
- [127] S. Huang, L. Liu, Y. Zheng, Y. Wang, D. Kong, Y. Zhang, Y. Shi, L. Zhang, O. G. Schmidt, H. Y. Yang, *Adv. Mater.* **2018**, *30*, 20.
- [128] C. H. Lim, T. Y. Huang, P. S. Shao, J. H. Chien, Y. T. Weng, H. F. Huang, B. J. Hwang, N. L. Wu, *Electrochim. Acta* **2016**, *211*, 265.
- [129] C. Yue, Y. Yu, S. Sun, X. He, B. Chen, W. Lin, B. Xu, M. Zheng, S. Wu, J. Li, J. Kang, L. Lin, *Adv. Funct. Mater.* **2015**, *25*, 1386.
- [130] C. Chandra, W. Devina, A. D. M. Sarofil, J. Kim, *Chem. Eng. J.* **2022**, *438*.
- [131] M. Winter, B. Barnett, K. Xu, *Chem. Rev.* **2018**, *118*, 11433.
- [132] W. Zhang, F. Zhang, F. Ming, H. N. Alshareef, *EnergyChem* **2019**, *1*, 100012.
- [133] C. Wang, L. Liu, S. Zhao, Y. Liu, Y. Yang, H. Yu, S. Lee, G. H. Lee, Y. M. Kang, R. Liu, F. Li, J. Chen, *Nat. Commun.* **2021**, *12*, 2256.
- [134] W. Zuo, X. Liu, J. Qiu, D. Zhang, Z. Xiao, J. Xie, F. Ren, J. Wang, Y. Li, G. F. Ortiz, W. Wen, S. Wu, M. S. Wang, R. Fu, Y. Yang, *Nat. Commun.* **2021**, *12*, 1.
- [135] E. A. Wu, S. Baner, E. A. Wu, S. Banerjee, H. Tang, P. M. Richardson, J.-M. Doux, J. Qi, Z. Zhu, A. Grenier, Y. Li, E. Zhao, G. Deysher, E. Sehti, H. Nguyen, R. Stephens, G. Verbist, K. W. Chapman, R. J. Clément, A. Banerjee, Y. S. Meng, S. P. Ongjee, *Nat. Commun.* **2021**, *12*, 1.
- [136] X. Shen, Q. Zhou, M. Han, X. Qi, B. Li, Q. Zhang, J. Zhao, C. Yang, H. Liu, Y. S. Hu, *Nat. Commun.* **2021**, *12*, 1.
- [137] Q. Shi, R. Qi, X. Feng, J. Wang, Y. Li, Z. Yao, X. Wang, Q. Li, X. Lu, J. Zhang, Y. Zhao, *Nat. Commun.* **2022**, *13*, 1.
- [138] H. Kim, H. Kim, Z. Ding, M. H. Lee, K. Lim, G. Yoon, K. Kang, *Adv. Energy Mater.* **2016**, *6*, 1600943.
- [139] A. V. Baskar, G. Singh, A. M. Ruban, J. M. Davidraj, R. Bahadur, P. Sooriyakumar, P. Kumar, A. Karakoti, J. Yi, A. Vinu, *Adv. Funct. Mater.* **2022**, *33*, 2208349.
- [140] M.-M. Xie, Z. Xu, Z. Guo, F. Titirici, *Progress in Energy* **2020**, *2*, 042002.
- [141] S. Dou, I. Hasa, D. Saurel, C. Vaalma, L. Wu, D. Buchholz, D. Bresser, S. Komaba, X. Passerini, *Mater. Today* **2019**, *23*, 87.
- [142] S. Wahid, D. Puthusseri, Y. Gawli, N. Sharma, M. Ogale, *ChemSusChem* **2018**, *11*, 506.
- [143] J. R. Fitzpatrick, S. I. R. Costa, N. Tapia-Rui, *Johnson Matthey Technology Review* **2022**, *66*, 44.
- [144] Z. Liang, F. Tian, G. Yang, C. Wang, *Nat. Commun.* **2023**, *14*, 3591.
- [145] Y. Jin, P. M. L. Le, P. Gao, Y. Xu, B. Xiao, M. H. Engelhard, X. Cao, T. D. Vo, J. Hu, L. Zhong, B. E. Matthews, R. Yi, C. Wang, X. Li, J. Liu, J. G. Zhang, *Nat. Energy* **2022**, *7*, 718.
- [146] Z. Deng, T. P. Mishra, E. Mahayoni, Q. Ma, A. J. K. Tieu, O. Guillon, J. N. Chotard, V. Seznec, A. K. Cheetham, C. Masquelier, G. S. Gautam, P. Canepa, *Nat. Commun.* **2022**, *13*, 4470.
- [147] D. A. Rakov, F. Chen, S. A. Ferdousi, H. Li, T. Pathirana, A. N. Simonov, P. C. Howlett, R. Atkin, M. Forsyth, *Nat. Mater.* **2020**, *19*, 1096.
- [148] X. Wang, C. Zhang, M. Sawczyk, J. Sun, Q. Yuan, F. Chen, T. C. Mendes, P. C. Howlett, C. Fu, Y. Wang, X. Tan, D. J. Searles, P. Král, C. J. Hawker, A. K. Whittaker, M. Forsyth, *Nat. Mater.* **2022**.
- [149] H.-Q. Gong, X.-Y. Wang, L. Ye, B. Zhang, X. Ou, *Tungsten* **2023**.
- [150] R. Ramadan, M. Manso-Silván, R. J. Martín-Palma, *J. Mater. Sci.* **2020**, *55*, 5458.
- [151] Z. Li, L. Ma, T. W. Surta, C. Bommier, Z. Jian, Z. Xing, W. F. Stickle, M. Dolgos, K. Amine, J. Lu, T. Wu, X. Ji, *ACS Energy Lett.* **2016**, *1*, 395.
- [152] X. Han, Z. Li, F. Yang, Z. Xiao, Y. Yu, G. Ning, L. Jia, *Powder Technol.* **2021**, *382*, 541.
- [153] A. Agrawal, K. Biswas, S. K. Srivastava, S. Ghosh, *J. Solid State Electrochem.* **2018**, *22*, 3443.
- [154] Y. Feng, L. Liu, X. Liu, Y. Teng, Y. Li, Y. Guo, Y. Zhu, X. Wang, Y. Chao, *Electrochim. Acta* **2020**, *359*, 136933.



Alireza Fereydooni received a Master of Science in the field of chemical engineering in 2022 from Sharif University of Technology, Iran. Presently, he is pursuing a Ph.D. in nanotechnology at the University of East Anglia, the United Kingdom. Among his research interests are the design and implementation of sustainable materials for use as anodes in high-performance batteries, and their role in large-scale decarbonization.



Chenghao Yue received his PhD in 2020 and is currently working as a senior research associate in University of East Anglia, the United Kingdom. He passionately explores nano materials, particularly focusing on the advanced silicon anode technology for lithium-ion batteries.



Yimin Chao was appointed as a Reader in the School of Chemistry at University of East Anglia on the basis of an established track record in investigating nanostructured systems from the basic physical and chemical mechanisms of synthesis, through their optical and electronic properties to scientific and industrial applications in environmental and energy storage systems. He is a Fellow of Royal Society of Chemistry, Secretary of Chemical Nanoscience and Nanotechnology Network. He is serving as a member of UKRI Future Leaders Fellowships Panel and EPSRC Peer Review College.